Fluorescence and absorption studies of $Sr_{0.999-x}Gd_{0.001}Ce_xF_{2.001+x}$ †

Perry Pappas Yaney, D. Michael Schaeffer,*‡ and James L. Wolf§‡
The University of Dayton, Dayton, Ohio 45469
(Received 29 July 1974)

Cerium-concentration-dependence studies of the optical spectra of doubly doped SrF_2 with 0.1-mole% Gd^{3+} for eight Ce^{3+} concentrations ranging from 0.001 to 1.0 mole% were carried out. A new four-line pattern was observed in the $^6P_{7/2}$ fluorescence spectra of these samples. In addition, an unusual single-line spectrum was found in the $^6P_{7/2}$ region. These and other new features studied using intensity and lifetime measurements were tentatively identified as arising from various Gd-Ce mixed double and triple clusters. From the enhancement of the Gd fluorescence due to Ce at low Ce concentrations ($\lesssim$ 0.1 mole%) and other data, energy transfer from the Ce ion to the Gd ion in these clusters by exchange is proposed. The $^6P_{7/2}$ fluorescence excitation and decay scheme of the usual C_{4v} site was found to be the usual three-level scheme. The lifetime of the ^6I pump state was observed to be 13.5 msec ± 9% while for the $^6P_{7/2}$ decay we observed radiation trapping giving lifetimes as much as four times the radiative value of 10 msec. Analysis of the absorption spectra gave a self-consistent set of site concentrations vs Ce concentration for the O_h, C_{4v}, and C_{3v} sites of Gd. We observed an anomalous increase in the O_h site concentration with a corresponding decrease in the axial site concentration with increasing Ce concentration starting at about 0.1-mole% Ce. An *ad hoc gettering* model is proposed which assumes that the Ce ions extract extra interstitial F^- ions from the Gd population producing the observed site-concentration changes. The calculations based on this model provide a satisfactory fit to the observed data.

I. INTRODUCTION

One of the most interesting features of the study of rare-earth ions in the fluorite lattice (e.g., Ca, Sr, and BaF_2) is the multiplicity of site symmetries available to the rare-earth ion.[1] These various sites rise out of the scheme by which the additional charge on the trivalent rare-earth ion is compensated in the divalent fluorite host. The most common site symmetries are cubic (O_h), tetragonal (C_{4v}), and trigonal (C_{3v}). Needless to say, this greatly complicates the observed spectra. On the other hand, once the spectra are analyzed, these systems offer a wealth of opportunities to investigate crystal-field splittings,[2,3] intensities of crystal spectra,[4] ion-lattice interactions,[5] molecular-orbital contributions,[6] and defect structures in impure (i.e., doped) crystals.[7,8]

A number of optical studies have been performed on the excited states of Gd^{3+} in the SrF_2 lattice which have yielded the site identity of most of the commonly observed lines. Gilfanov *et al.*[9] and Makovsky[10] independently identified the lines belonging to the O_h, C_{4v}, and C_{3v} sites. The O_h site in CaF_2[11,12] and SrF_2[13] the C_{4v} site in SrF_2[13] have been verified in Zeeman studies. The line groupings according to common sites in SrF_2 have been verified quantitatively by Ferralli and Yaney[14] and Detrio *et al.*[15] using concentration studies in absorption and by Smith and Yaney[16] using concentration studies in fluorescence. A somewhat unique aspect to the optical study of Gd^{3+} spectra compared to other impurity-ion spectra is the fact that the ground-state crystal-field splitting is extremely small, being on the order of or less than one wave number.[17] Thus, the line patterns observed in the optical spectra are due entirely to crystal-field-induced splittings of the excited states. This greatly simplifies the experimental studies, particularly of the first two excited states, namely, the $^6P_{7/2}$ and $^6P_{5/2}$ states. Group theory shows that all axial sites will give four and three line patterns for these two states, respectively, whereas a cubic site gives distinctive three- and two-line patterns, respectively.

Studies of energy transfer to Gd^{3+} (the activator) from another rare-earth codopant (the sensitizer) has received no attention due to the fact that the Gd^{3+} spectrum lies in the quartz and vacuum-ultraviolet regions. Laser action from Gd^{3+} has been reported[18] only once and, to our knowledge, has never been confirmed. Livanova *et al.*[19] have studied energy transfer from Gd^{3+} to Pr^{3+} in CaF_2. For the most part, however, gadolinium has been used as a nonabsorbing host ion for which other rare earths can be substitutionally added.[20,21]

On the other hand, Ce^{3+} has been used as a sensitizer in numerous laser studies,[22] and it has also shown considerable promise as an activator in phosphors.[23] As a sensitizer, it has, in some cases, been found to quench the fluorescence[22,24] of the activator either due to a draining off of the activator energy to a lower-lying nonfluorescent state via resonance transfer to the $^2F_{7/2}$ state of its $4f$ configuration, or simply by the competition with its fast[25] (~0.1 μsec) $5d$ to $4f$ fluorescence decay. Figure 1 shows the energy-level diagrams of Gd^{3+} and Ce^{3+} in SrF_2. Because

of this fast decay, there would seem little probability of enhancing the Gd^{3+} fluorescence with the addition of Ce^{3+}. Nevertheless, the low-resolution excitation spectra of Gd^{3+} plus Ce^{3+} in SrF_2 given in Fig. 2 shows that the $^6P_{7/2}$ fluorescence is excited by 2500-Å radiation as well as by 2750 Å. From Fig. 1 is clear that the 2750-Å excitation arises from the absorption into the ^6I manifold, and it would appear that the 2500-Å excitation comes from the ^6D absorption. However, Gilfanov *et al.*[26] have reported that no $^6P_{7/2}$ fluorescence was observed in their samples when the ^6D manifold was pumped. The weak oscillator strengths of the ^6D lines fully support that observation. Also, Fig. 2 as well as higher-resolution excitation spectra show that the fluorescence in the region of 3000 to beyond 3500 Å was pumped not only by the 2500-Å band but also by a band centered around 2950-Å which coincides with the low-lying absorption band of Ce^{3+} in Fig. 1. The short-wavelength edge of this band is evident in Fig. 2. A similar examination of the spectra of a single-crystal sample of the pure SrF_2 material used in our doped samples revealed the same 2500- and 2950-Å excitation bands. Thus, by comparing these results to the Ce^{3+} spectra summarized in Fig. 1, it was strongly suggested that the SrF_2

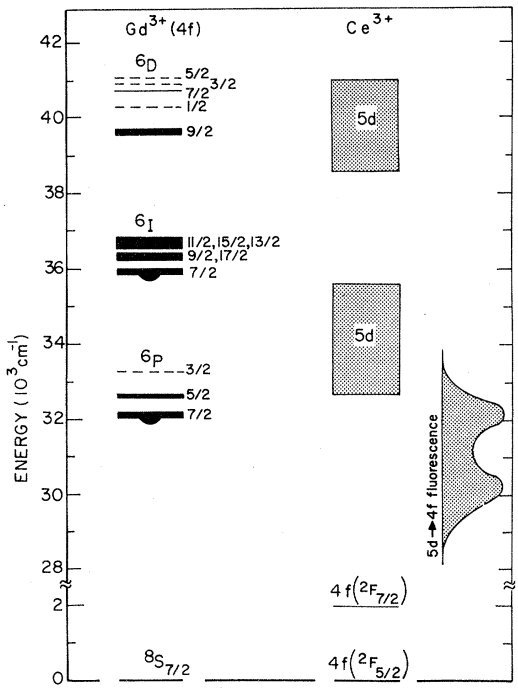

FIG. 1. Energy levels of Gd^{3+} and Ce^{3+} in SrF_2. The pendant half-circles indicate levels from which fluorescence is observed, and the dashed lines indicate unobserved states.

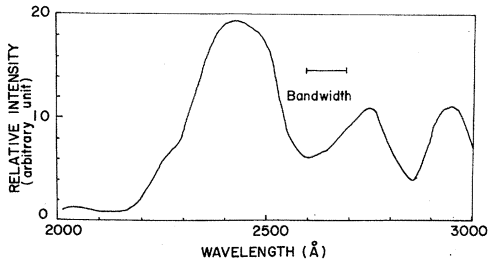

FIG. 2. Excitation spectrum of the $^6P_{7/2}$ levels of Gd^{3+} in SrF_2(0.1-mole% Gd^{3+} + 0.2-mole% Ce^{3+}) at 77 °K.

material contained a trace of Ce^{3+} and that this was responsible for the enhancement of the $^6P_{7/2}$ emission in the Gd^{3+}-doped samples under 2500-Å excitation. Since these spectra did not resolve the lines of the $^6P_{7/2}$ state belonging to the various sites, it was necessary to do high-resolution absorption and fluorescence studies as a function of Ce^{3+} concentration in order to ascertain which site was being enhanced. Lifetime measurements of the fluorescence decay of the observed lines were also performed to aid in the determination of the decay schemes of the two most prevalent sites. The two sites are the common C_{4v} site and a new site that is enhanced or created by the cerium doping which we label the *GC*1 site. We argue that this new site is due to the clustering of Gd^{3+}, F^-, and Ce^{3+} ions to give an orthorhombic site and that the observed energy transfer is by exchange. In addition, we attempt to suggest origins for the curious appearance of a one-line spectrum and of lines which grow rapidly with the cerium concentration.

By a detailed analysis of the absorption and fluorescence spectra, we also attempt to provide a different viewpoint regarding the question of locally versus nonlocally compensated cubic sites in doubly doped samples.[27,28] The cubic site cited at the beginning of this section and the one observed in this study are assumed to be of the same origin and, as is customary, it will be referred to as a singly F^- compensated site where it is understood that the F^-_{int} ion is beyond the third-nearest-neighbor interstitial position.

II. EXPERIMENTAL TECHNIQUES

A. Samples

The samples used in this study were single-crystalline SrF_2 doped with Gd^{3+} and Ce^{3+} and were prepared[29] by the Stockbarger-Bridgemann method under essentially identical conditions in a high vacuum with PbF_2 added as a scavenging agent to eliminate hydrolysis products. All samples were fabricated into right circular

cylinders, the height and diameter of which were both approximately 10 mm and were polished to a plate-glass finish on all surfaces. Ten samples were used in this investigation and are designated by SrF_2(y-mole% Gd^{3+} +x-mole% Ce^{3+}). The superscripts 3+ will be dropped hereafter in the text since only the trivalent species of these ions are discussed. Eight of the samples were doubly doped with y being nominally constant at 0.1 and with the following values of x: 0.001, 0.01, 0.02, 0.05, 0.1, 0.2, 0.5, and 1.0. The remaining two samples were singly doped with $x = 0.01$ (and $y = 0$) in one and $y = 0.1$ (and $x = 0$) in the other. Hereafter, all concentration percentages will refer to the molar values.

The dopings reported above were the nominal concentrations supplied by the manufacturer and were checked through spectrochemical analysis.[30] Unfortunately, except for the higher cerium concentration samples, the sensitivity of the cerium analysis was insufficient, resulting in large scatter in the numerical data. The same situation existed for the gadolinium analysis but to a lesser degree. However, previous experience in comparing the supplier's nominal doping levels to spectrochemical analyses at higher doping levels has indicated that the nominal level is accurate to at least ±30%. The results of the sample-to-sample intensity measurements presented in Sec. III show fairly smooth changing relationships with cerium concentration supporting the claim that at least the relative concentrations are reasonably given by the nominal levels. The only exception to this is the SrF_2 (0.1% Gd +0.2% Ce) sample for which the measurements suggested that the Gd concentration was actually about 1.5 times that in the other doubly doped samples.

B. Spectroscopic measurements

High-resolution absorption spectra were obtained from a Jarrell-Ash, 3.4-m focal length, Ebert mount, grating spectrograph. It was fitted with a Bausch and Lomb 1800-grooves/mm grating which was used in second order, giving a linear reciprocal dispersion of approximately 0.7 Å/mm and a theoretical resolving power of 440 000 at 3100 Å. A slit width of 20 μm, approximately twice the diffraction limit of the instrument, was used. This provided an observed effective spectral width of 0.15 cm^{-1} at the focal plane which corresponds to a factor of roughly $\frac{1}{7}$th of the narrowest Gd absorption line in the ^6P_J region. Selected doubly doped samples ($x = 0.01$, 0.1, 0.2, 0.5, and 1.0) were chosen for high-resolution-absorption studies in the ^6P_J multiplet and were examined at 77 °K only. The absorption spectrum was produced using a 900-W Osram high-pressure compact-arc Xe lamp.

High-resolution fluorescence spectra were also photographed using the 3.4-m spectrograph. To admit more light into the spectrograph and to minimize long exposure times, the slit width was increased to 50 μm, which corresponds to an effective slit width of approximately 0.35 cm^{-1} on the plates and is roughly a factor of 3 smaller than the narrowest fluorescence transition in the $^6P_{7/2}$ manifold. Excitation of the fluorescence was accomplished using either a 900-W forced-air-cooled Hg-capillary lamp, G. E. type BH-6, or a 1000-W high-pressure compact-arc Hg-Xe lamp, Hanovia type 977-B1, and a 0.25-m Jarrell-Ash monochromator set to give about 100-Å spectral width.

The absorption spectra were photographed on Kodak V-F plates and the fluorescence spectra, on Kodak 103a-O plates. Wavelength calibration was accomplished with a Westinghouse Fe-Ne hollow cathode lamp and the optical density vs exposure characteristic was obtained with a seven-step calibrated neutral density filter at the entrance slit of the spectrograph. The plates were traced on a Joyce-Loebl Mark IIB microdensitometer.

A study of the $^6P_{7/2}$ fluorescence in all samples under 2500- and 2750-Å excitations was also made using a 2.25-m focal length, Jarrell-Ash, Ebert-Fastie mount, spectrograph fitted with an 1180-grooves/mm grating in first order and equipped with a photomultiplier scanning attachment. An effective slit width of approximately 1 Å was used. Such a width is wide enough so that the maximum fluorescence intensity recorded for a given line was proportional to the integrated intensity of that line, but narrow enough to resolve the individual lines within the spectra of most of the samples.

C. Lifetime measurements

In lifetime studies, the excitation optics must provide a means of turning the excitation light on and off, since the fluorescence decay can be observed only during the off interval. A simple method for chopping the excitation is to place a driven chopper wheel at the focus of the excitation beam. In the construction of such excitation optics, the excitation source and the monochromator assembly are chosen to complement the operation of the mechanical chopper. The two lamps cited, the 977-B1 and the BH-6, were both considered for use as the source of uv excitation. The 977-B1 lamp was preferred to the BH-6 lamp because its output at 2500 Å is about equal to its 2750-Å output, which is not the case for the BH-6 lamp and for the following geometrical

considerations. The BH-6 lamp can be focused to the linear dimensions of the monochromator slit, whereas the 977-B1 lamp produces a small circular image of its arc. The advantage of the latter is that the chopper wheel evenly cuts off the excitation beam, but due to its geometry, a line source of finite width cannot be evenly chopped by a circular disk in a straightforward manner.

The chopper assembly consisted of a single-blade chopper wheel mounted on an 1800-rpm synchronous motor giving an excitation chopping rate of 30 Hz. The maximum tangential velocity on the chopper wheel is at a point radially farthest from its center. Thus, to achieve the fastest possible cutoff of the excitation, the chopper was placed as closely as possible to the monochromator entrance slit on which the arc was focused and at a point where the edge of wheel traversed the arc image. The entrance slit fixes the excitation cutoff time. Experimentally, the excitation cutoff was completed in 0.2 msec with a 2-mm slit width with this arrangement, which limited the measurement of lifetimes to those longer than about 2 msec. While a smaller entrance slit lowered the cutoff time, it decreased the light intensity incident on the sample. Using the SrF_2(0.1%Gd+0.1%Ce) sample from which the largest fluorescence output was detected in the $^6P_{7/2}$ transitions of the $GC1$ site, a cutoff time as low as 80 μsec was obtained without severe loss of signal-to-noise ratio, when the entrance slit was narrowed to approximately 1 mm. The 2-mm entrance slit, however, was found to be a good compromise between a high single-to-noise ratio and a fast chopper cutoff.

The fluorescence was analyzed spectrally using a 0.25-m Jarrell-Ash monochromator similar to the one used in the excitation optics. Since its speed $f/40$ was too slow, the 2.25-m spectrograph equipped with the photomultiplier provided too weak a signal for lifetime measurements. The fluorescence decay from all levels belonging to a particular $^6P_{7/2}$ site, the maximum splitting of which was approximately 8 Å, was observed simultaneously in these measurements. The detector used in the photoelectric measurements was an uncooled 1P28. The decay curves were recorded using a PAR CW-1 boxcar integrator. The exponential decay was linearized using a Burr-Brown log-ratio converter and recorded in both analog and digital forms. The lifetimes were calculated by computer using a least-squares fit.

III. RESULTS

A. Absorption spectra

A composite of the $^6P_{7/2}$ absorption spectra recorded at high resolution for five of the doubly doped samples is shown in Fig. 3. The line patterns

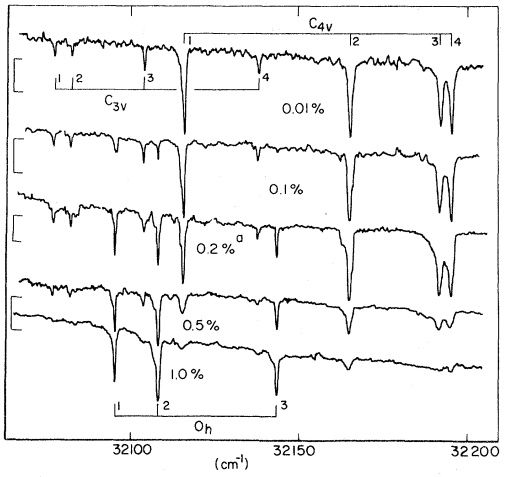

FIG. 3. Densitometric traces of the $^6P_{7/2}$ absorption spectra of 0.1-mole% Gd^{3+} in double-doped SrF_2 at 77 °K where the Ce^{3+} molar concentrations x are given in the figure. See text concerning the site indentifications. The brackets on the left correspond to an absorption coefficient increment of 0.05 cm^{-1}. (a) This spectrum indicates that this sample has a Gd^{3+} concentration about 1.5 times higher than in the other samples.

are characteristic of the three usual fluorine-compensated Gd sites reported by Makovsky[10] and Gilfanov *et al.*,[9] namely, the trigonal, tetragonal, and cubic sites referred to in Sec. I. The concentration studies of Ferralli and Yaney[14] and Detrio *et al.*[15] on Gd-doped SrF_2 showed that the concentrations of these sites increase with increasing Gd concentration (although at different rates). However, the spectra in Fig. 3 clearly show that only the cubic spectrum increases with Ce concentration, with the tetragonal and trigonal sites nearly absenct at the 1%-Ce doping level. This result was also reported in the EPR spectra of these sites in these samples.[27] The positions of these lines and of the $^6P_{5/2}$ lines are summarized in Table I for the SrF_2(0.1%Gd+0.2%Ce) sample. The positions of these lines in the remaining samples were, on the average, within ±0.03 cm^{-1} of the of the values given in Table I and showed no systematic shifts. The low-resolution absorption spectra in the near-uv of selected samples are given in Fig. 4. These spectra, reported by Kaplyanskii *et al.*[31] and by Loh,[32] show that for our samples the broad $4f$-$5d$ bands due to Ce increase in reasonable accord with the increase in the nominal Ce concentration.

Optical-absorption spectra provide a means of obtaining the absolute concentrations of the impurity sites providing the strengths of the transitions are known. In sites having inversion symmetry, such as the cubic site, transitions between states belonging to the $4f$ configuration

TABLE I. Air wavelengths and vacuum wavenumbers of $^8S_{7/2} \rightarrow {}^6P_J$ absorption transitions of Gd^{3+} in SrF_2 (0.1-mole % Gd^{3+} + 0.2-mole % Ce^{3+}). [a]

Line	λ(Å)	ν(cm^{-1})
	$^6P_{7/2}$	
$A_1(C_{3v})$	3116.57	32 077.3
$A_2(C_{3v})$	3116.09	32 082.2
$A_3(O_h)$	3114.79	32 095.6
$A_4(C_{3v})$	3113.98	32 104.0
$A_5(O_h)$	3113.54	32 108.5
$A_6(C_{4v})$	3112.83	32 115.8
$A_7(C_{3v})$	3110.71	32 137.7
$A_8(O_h)$	3110.17	32 143.3
$A_9(C_{4v})$	3108.07	32 165.0
$A_{10}(C_{4v})$	3105.50	32 191.6
$A_{11}(C_{4v})$	3105.16	32 195.1
	$^6P_{5/2}$	
$B_1(C_{3v})$	3059.42	32 676.4
$B_2(C_{3v})$	3058.80	32 683.1
$B_3(O_h)$	3057.57	32 696.3
$B_4(C_{3v})$	3056.88	32 703.6
$B_5(O_h)$	3056.02	32 712.8
$B_6(C_{4v})$	3054.40	32 730.2
$B_7(C_{4v})$	3050.94	32 767.2
$B_8(C_{4v})$	3050.02	32 777.2

[a] Line identification symbols are those used by Ferralli and Yaney (Ref. 14) and Detrio *et al.* (Ref. 15). See text regarding symmetry assignments.

are restricted to interactions involving no change in parity, namely, magnetic dipole and electric quadrupole. This comes from the fact that a cubic crystal field does not have any odd-parity electrostatic crystal-field terms which can mix, through second-order perturbations, configurations of opposite parity with the $4f$ configuration. In general for any site, the oscillator strength f and the site fraction ϵ are related to the measured absorption coefficient $k(\nu)$ in cm^{-1} by

$$\epsilon f = 2(\alpha \lambda_c N_y)^{-1} \int k(\nu)\, d\nu \,, \qquad (1)$$

where α is the fine-structure constant, λ_c is the Compton wavelength of the electron, N_y is the density of Gd ions in cm^{-3}, ν is the frequency in cm^{-1}, and the integration extends over all the lines of a given J manifold belonging to a given site. Since for the ^6P_J states of Gd the electric quadrupole strength is negligible,[4] then for the cubic site the fraction of Gd ions in that site can be determined from the total integrated absorption coefficient $\int k(\nu) d\nu$ and the calculated magnetic dipole oscillator strength f_m.

The total magnetic dipole oscillator strength calculated on the intermediate-coupled basis ($[\tau SLJ]$) between two J manifolds is given by

$$f_m = \eta \alpha^2 \nu [12 R_\infty (2J+1)]^{-1} \times | ([\tau SLJ] \| M^{(1)} \| [\tau' S' L' J']) |^2 , \qquad (2)$$

where R_∞ is the Rydberg constant, η is the index of refraction, τ, S, L, J and τ', S', L', J' are the usual quantum numbers needed to specify the Russell-Saunders ground and excited basis states, respectively, and $M^{(1)}$ is the magnetic dipole tensor operator of the form $M^{(1)} = \sum (L^{(1)} + g_s S^{(1)})$ (summed over all electrons).

The values obtained, due to differing amounts of J mixing, depend on the basis chosen. The values for the $^6P_{7/2}$ and $^6P_{5/2}$ states are 6.35 and 3.58 $\times 10^{-8}$ for the free-ion basis, 6.41 and 3.53×10^{-8} for the cubic basis, and 6.59 and 3.62×10^{-8} for the tetragonal basis, respectively.[4] Thus, for the cubic case, a self-consistent estimate of the cubic site concentrations can be obtained directly using the above cubic values and the observed integrated absorption in Eq. (1).

The axial sites of interest, on the other hand, lack inversion symmetry, and therefore, have nonzero values of the odd-parity electrostatic crystal-field coefficients. These coefficients allow opposite parity configurations to mix with the $4f$ configuration, thereby permitting electric dipole transitions to take place. The axial-site spectra, then, contain a mixture of magnetic and electric dipole transitions. In this case, the total electric dipole oscillator strength f_e between two J manifolds can be written as[33]

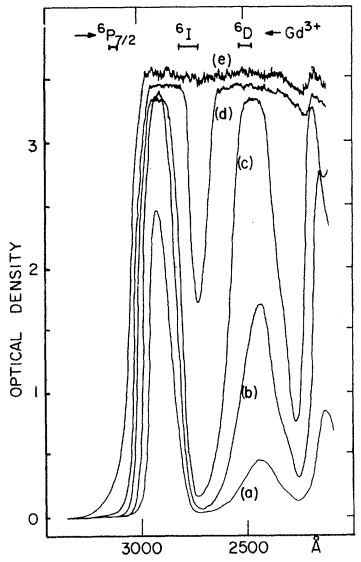

FIG. 4. Absorbance spectra of SrF_2 (0.1-mole% Gd^{3+} + x-mole% Ce^{3+}) at room temperature where x is (a) 0.01, (b) 0.02, (c) 0.1, (d) 0.5, and (e) 1.0.

$$f_e = \sum_{t=2,4,6} [\nu \chi T^{(t)}/(2J+1)] \times |([\tau S L J] \| U^{(t)} \| [\tau' S' L' J'])|^2 , \quad (3)$$

where χ is a correction factor due to the polarizability of the medium, $T^{(t)}$ are parameters representing the strength of the coupling produced by the odd-parity terms, and $U^{(t)}$ are the unit-tensor operators. Since the parameters L, t, and L' must fulfill the triangle rule,[33] then the electric dipole portions of the $^8S_{7/2} \rightarrow {}^6P_{7/2}$, $^6P_{5/2}$ transitions are characterized primarily by $t=2$ arising from the ^6P content of the $[^8S]$ state. Thus, the total strength for an axial site is just the sum of Eq. (3), for $t=2$, and Eq. (2). The difficulty in performing this calculation is that $T^{(2)}$ must be determined. However, since we know the magnetic dipole strength, the only unknowns are the electric dipole contributions to the two states and the site fraction. The experimental data provide two values of ϵf, one for each state. Examination of Eq. (3) for this case shows that the ratio of the electric dipole strengths for transitions to the two states can be calculated. This ratio is given by

$$r_e \equiv f_{eB}/f_{eA} = \frac{(\nu_B/\nu_A)|([^8S] \| U^{(2)} \| [B])|^2}{|([^8S] \| U^{(2)} \| [A])|^2} , \quad (4)$$

where, for the free-ion case,

$$r_e = (32\,758.4/32\,166.6)(-0.021\,72/0.034\,01)^2 = 0.4154,$$

the values for ν_A and ν_B are the centers of energy, and A and B denote the $^6P_{7/2}$ and $^6P_{5/2}$ manifolds of levels, respectively. This ratio reduces the number of electric dipole contributions required to one, thereby providing a means of determining the transition strengths and site fractions of axial sites from the experimental data.

Basically, the axial-site problem reduces to two equations in two unknowns. Inasmuch as the electric and magnetic dipole operators are independent, then if the strengths of all the transitions between two J manifolds are summed over the quantum numbers M_J of the projection J_z of the J's belonging to the two states, the total strength f is given by

$$f = f_m + f_e .$$

Since the quantity obtained from experiment for a site is ϵf given by Eq. (1), then for states A and B we have, in general,

$$(\epsilon f)_A = \epsilon (f_{mA} + f_{eA})$$

and

$$(\epsilon f)_B = \epsilon (f_{mB} + f_{eB}) .$$

Manipulating these expressions, using Eq. (4), we obtain the measured total oscillator strength to state A as

$$f_A = f_{mA}[(r_m - r_e)/(\bar{R} - r_e)] , \quad (5)$$

where the ratio of magnetic dipole contributions is

$$r_m \equiv f_{mB}/f_{mA} ,$$

and the average ratio of the experimental strengths is

$$\bar{R} \equiv n^{-1} \sum_i (\epsilon f)_{B_i}/(\epsilon f)_{A_i} ,$$

summed over n samples. The site fraction of the ith sample is found from

$$\epsilon_i = (\epsilon f)_{A_i}/f_A ,$$

and the measured total oscillator strength to state B is given by

$$f_B = n^{-1} \sum_i (\epsilon f)_{B_i}/\epsilon_i ,$$

summed over n samples. It is important to note that the quantity in the brackets of Eq. (5) is sensitive to the value of r_m, whereas it is rather insensitive to the value of r_e. Thus, we are justified in using the free-ion value for r_e; however, the values of r_m are 0.5638, 0.5507, and 0.5493 for the free-ion, cubic, and tetragonal cases, respectively.[4] Using the free-ion values in Eq. (5) gives for $10^8 f_A$ and $10^8 f_B$, respectively, 7.6 and 4.1 as compared to 7.1 and 3.9 with tetragonal values. The latter are in better accord with those found by Detrio.[4]

The results obtained for the tetragonal site using the tetragonal values for f_m and r_m from this procedure are given in Table II. The estimated site concentrations for the trigonal and cubic sites are also given. These values were obtained by dividing the total of the (ϵf)'s for the A and B groups belonging to the site by the total calculated oscillator strength, for that site. For the cubic site, assuming the transitions are totally magnetic dipole, the strength used was 9.94×10^{-8}. For the trigonal site, the average of this value with that obtained for the tetragonal site was used, namely, 10.1×10^{-8}. This is a reasonable estimate since the electric dipole contributions to the transitions in the trigonal site would be less than those in the tetragonal site due to the larger separation between the Gd ion and the charge-compensating F^- ion in the trigonal site compared to that in the tetragonal site. It was not possible to arrive at a more precise estimate of the trigonal oscillator strengths using the fitting procedure described above because

TABLE II. Estimated site fractions ϵ_y and oscillator strengths f calculated from the $^6P_{7/2}$ (A) and $^6P_{5/2}$ (B) integrated absorption coefficients of Gd^{3+} in the SrF_2 (0.1-mole % Gd^{3+} + x-mole % Ce^{3+}) samples. [a]

Site	x	$10^8(\epsilon_y f)_A$	$10^8(\epsilon_y f)_B$	ϵ_y (%)	$10^8 f$ A	B
C_{4v}	0	4.6	2.6	65		
	0.01	3.9	2.1	55		
	0.1	3.5	1.8	49		
	0.2	4.3	2.4	40 [b]	7.1 ±10%	3.9
	0.5	1.5	0.92	21		
	1.0	0.45	0.21	6		
O_h	0	~0		<1		
	0.1	~0.4		~4		
	0.2	1.9		13 [b]	6.41 [c]	3.53 [c]
	0.5	2.0		20		
	1.0	2.7		27		
C_{3v}	0	1.5		15		
	0.01	0.83		8		
	0.1	0.51		5	10.1 (total)	
	0.2	1.1		7 [b]		
	1.0	~0		<1		

[a] See text for details of calculation.

[b] The ϵf values for the 0.2% Ce sample have been divided by 1.5 to account for its Gd^{3+} concentration being higher than in the remaining samples in the calculation of ϵ_y.

[c] Values after Detrio (Ref. 4).

of the weak strengths in the trigonal spectra.

The tetragonal data, on the other hand, for the first four samples showed remarkable agreement with the data for the tetragonal site in singly doped SrF_2.[4] In the latter case, the observed ratio of strengths was found to be $\bar{R} = 0.542 \pm 1.3\%$. The first four samples in Table II have reasonable strengths in the tetragonal spectra for which we obtained a ratio of $\bar{R} = 0.54 \pm 4\%$. This is the value used in computing f_A in Eq. (5). The tetragonal site fractions are estimated to be self-consistent to within ±5%, where the actual site fraction may differ due to a systematic shift of the actual Gd concentration in the samples from the 0.1% nominal value. The electric dipole contributions are estimated to be 0.5×10^{-8} and 0.3×10^{-8}, both ±50%, for the A and B transitions, respectively. This corresponds to a value for T_2 in Eq. (3) of about 9×10^{-10} cm, which is within a factor of 3 of that obtained by Detrio[4] for the singly doped samples.

The site fractions are plotted in Fig. 5 for the three sites with the total fraction also given versus the Ce concentration. The indicated dependences are in general agreement with the EPR measurements[27] on the samples with the highest Ce concentration showing 82% of the observed spectra belonging to the cubic site as compared to 85% obtained in EPR. The central distinction between Fig. 5 and the EPR results is that Fig. 5 shows the absolute concentration of Gd in a given F^--compensated site whereas the EPR study reports ratios of site intensity to total observed intensity. Table II shows that at low Ce concentrations about 20% of the Gd ions are not in the three singly F^- compensated sites. If the electric dipole contribution was one half of the value estimated above for the tetragonal site, this value would still be about 17%. It is reasonable to assume that part of this 20% of the rare-earth concentration in a fluorite is in various energetically favored cluster sites such as would be associated with vacancies or lattice dislocations. Another part of this fraction is probably due to the nominal 0.1%-Gd concentration being too high. Such a possibility is supported to some extent by spectrochemical analyses of the samples which often gave Gd concentrations between 0.05 and 0.07%. Another interesting feature of Fig. 5 is that the total site fraction curve can be divided into three distinct regions. The first ranges up to about 0.01% Ce, the second goes from 0.01 to 0.2% Ce, and the third region is above 0.2%. It is suggested that these regions correspond to the onset of a change in the cluster site fractions. This is discussed in more detail in the following subsections.

B. Fluorescence spectra

The high-resolution fluorescence spectra for three representative samples are shown in Fig. 6. The corresponding numerical data are presented in Table III. The excitation of the C_{4v} site takes place via absorption by the ^6I manifold of lines. Thus, its excitation is confined to the region around 2750 Å. Consistent with the absorption spectra, the C_{4v} site essentially disappears into the background at 1.0% Ce. It is replaced effec-

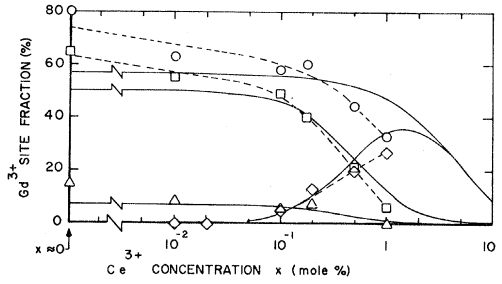

FIG. 5. The Ce^{3+} concentration dependences of the Gd^{3+} site fractions in SrF_2. The data points are experimental values obtained from the optical absorption data. The dashed curves were hand fitted to these points. See Table II and text. O_h site, ◇; C_{4v} site, □; C_{3v} site, △; total of the three sites, ○. The solid curves were calculated using the gettering model. See text.

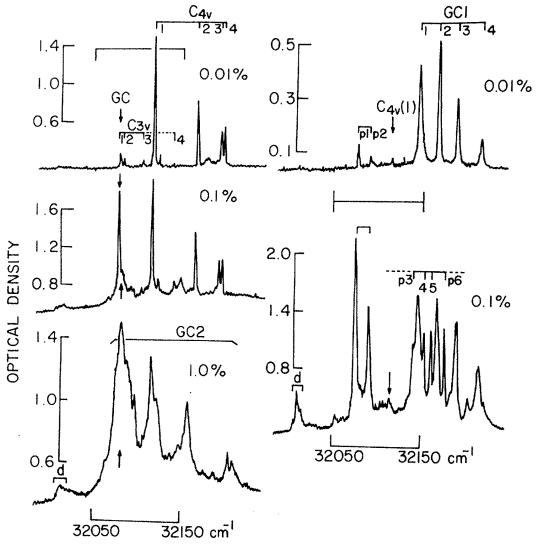

FIG. 6. Densitometric traces of the $^6P_{7/2}$ fluorescence spectra of 0.1-mole % Gd^{3+} in double-doped SrF_2 at 77 °K where the Ce^{3+} molar concentrations x are given in the figure. Traces at left are for 2750-Å excitation and traces at right are for 2500-Å excitation. See text concerning site identifications. The label d corresponds to the lines so labeled in Table III. The exposure conditions were not the same for these traces.

tively by a new group of broad lines which are labeled $GC2$.

A most interesting feature of the 2750-Å excitation spectra is the appearance of a single additional line on the low-wavenumber (i.e., long-wavelength) side of the C_{4v} site lines. This line occurs nominally at 32 078 cm^{-1}. A line occurs at 32 077 cm^{-1} with 2500-Å excitation also. Although low-wavenumber fluorescence lines have been observed in Gd-doped (singly) SrF_2 samples,[16,34] this particular line appears to be unique to the doubly doped samples. The excitation spectrum of this line in the 0.1% Ce doubly doped sample was found to have a peak at 2640 Å. The fluorescence spectrum in the $^6P_{7/2}$ region under 2600–2700-Å excitation showed a strong line centered at 32 077.5 cm^{-1} which is labeled GC. All other features were quite weak (by at least a factor of 10) compared to this line.

The fluorescence spectra observed with 2500-Å excitation is completely different than either the C_{4v} or the $GC2$ lines. Not only are the lines reasonably sharp, 3–6 cm^{-1}, but the overall splitting is 68 cm^{-1} compared to 61 cm^{-1} for the C_{3v} site and 80 cm^{-1} for the C_{4v} site (from Table I). The site responsible for these lines is labeled $GC1$. This four-line pattern appeared in all our low-Ce samples, including the singly doped Gd sample, with 2500-Å excitation. At high Ce concentrations, a number of additional sharp lines appeared in the spectra as shown, for example, in Fig. 6 for the 0.1% Ce sample the stronger of which we labeled $p1$ to $p6$. Three of these lines are almost coincident with the positions of two lines belonging to the C_{3v} site. Examining the relative intensities of these lines, especially with respect to the Boltzmann factor, and comparing their concentration dependence to that which would be predicted from Fig. 5, strongly suggests that these lines are not associated with the trigonal site. Because of their rapid growth with Ce concentration, it appears that these lines are due to clusters containing two Ce ions plus one or more Gd ions.

As can be seen in Fig. 6 and from Table III, the cubic and trigonal sites are weakly observed in fluorescence. This result is consistent with two facts. First, the concentrations of these two sites as given in Fig. 5 are quite low, particularly for the trigonal site. Second, since the cubic-site transitions obey magnetic dipole selection rules, then, from Fig. 1, only the $^6I_{7/2}$ and the $^6I_{9/2}$ states can absorb incident radiation as specified by the $\Delta J = 0, \pm 1$ selection rule. However, the only terms which will couple in Eq. (2) will be those where $\Delta S = 0$ and $\Delta L = 0$. Since the $^6I_{7/2}$ and $^6I_{9/2}$ content in the intermediate coupled ($[^8S]$| ground state is very small as well as the ^8S content in the ($[^6I_{7/2}]$| and ($[^6I_{9/2}]$| excited states,[2,3] then the excitation of cubic-site fluorescence is expected to be quite weak as observed. This circumstance also applies to the trigonal site since the electric dipole content of the transitions is insufficient for the trigonal ^6I absorption spectrum to appear in the singly doped 0.1% Gd sample.[14]

The Ce fluorescence spectrum in SrF_2 was shown by Kaplyanskii *et al.*[31] to consist of two broad bands, containing vibronic structure, both originating from the long-wavelength edge of the lowest absorption $5d$ band (about 3100 Å) with one terminating on the $^6F_{5/2}$ ground state and the other on the $^6F_{7/2}$ first excited state, both of the $4f$ configuration. This is illustrated in Fig. 1. These bands plus the sharp-line fluorescence from the $^6P_{7/2}$ state of Gd is shown in Fig. 7. The overlap of these lines with the Ce band gives rise to the possibility of resonant and near-resonant energy transfer from Ce to Gd. However, the extent to which such transfer occurs depends on the relative fluorescence lifetimes of the two ions and the transfer mechanism. In order to discern which processes were involved, we measured the Ce concentration dependence of the total Gd and total Ce fluorescence and of the fluorescence from the three line groups C_{4v}, $GC1$, and $GC2$. Graphical representations of these measurements are given in Figs. 8 and 9. Several conclusions can be drawn from these data. First of all, there is a signifi-

TABLE III. Vacuum wave numbers, relative peak intensities, and linewidths (FWHM) of the $^6P_{7/2}$ fluorescence spectra recorded photographically from the SrF_2 (0.1-mole % Gd^{3+} + x-mole % Ce^{3+}) samples under 2500-Å and 2750-Å excitations. [a]

x	ν (cm^{-1})	I_{max}	$\Delta\nu$ (cm^{-1})	Site [b]	Line [c]	x	ν (cm^{-1})	I_{max}	$\Delta\nu$ (cm^{-1})	Site [b]	Line [c]
	2750-Å Excitation						2500-Å Excitation				
0.01	32 195.2	0.26	2.1	C_{4v}	4	0.01	32 214.1	0.34	6.0	*GC*1	4
	32 191.9	0.24	2.9	C_{4v}	3		32 187.9	0.64	3.2	*GC*1	3
	32 165.2	0.41	1.9	C_{4v}	2		32 167.2	1.00	2.7	*GC*1	2
	32 122.6	*wi*	*wi*	∘∘∘	∘∘∘		32 145.9	0.98	5.4	*GC*1	1
	32 115.9	1.00	1.4	C_{4v}	1		32 115.3	≤0.17	*wi*	C_{4v}	1
	32 104.1	*wi*	*wi*	C_{3v}	3		32 091.8	≤0.17	*wi*	∘∘∘	*p*2
	32 082.6	*wi*	*wi*	C_{3v}	2		32 077.8	0.25	*wi*	∘∘∘	*p*1
	32 079.8	*wi*	*wi*	∘∘∘	∘∘∘	0.1	32 220.9	0.04	*wi*	∘∘∘	∘∘∘
	32 078.9	*wi*	*wi*	∘∘∘	∘∘∘		32 214.4	0.15	6.8	*GC*1	4
	32 078.4	*wi*	*wi*	∘∘∘	∘∘∘		32 212.6	0.12	*wi*	∘∘∘	∘∘∘
	32 077.8	*wi*	*wi*	∘∘∘	*GC*		32 203.0	0.09	*wi*	∘∘∘	∘∘∘
	32 077.3	*wi*	*wi*	C_{3v}	1		32 189.7	0.24	*wi*	∘∘∘	∘∘∘
0.1	32 194.8	0.35	*wi*	C_{4v}	4		32 188.6	0.24	5.0, *wi*	*GC*1	3
	32 191.6	0.35	*wi*	C_{4v}	3		32 175.9	0.20	3.6	∘∘∘	*p*6
	32 164.8	0.49	3.4	C_{4v}	2		32 169.4	0.33	*wi*	∘∘∘	∘∘∘
	32 148.4	0.27	*wi*	∘∘∘	∘∘∘		32 167.0	0.33	3.4, *wi*	*GC*1	2
	32 141.5	0.23	*wi*	∘∘∘	∘∘∘		32 161.0	0.23	3.7	∘∘∘	*p*5
	32 140.1	0.25	*wi*	∘∘∘	∘∘∘		32 153.2	0.22	3.7	∘∘∘	*p*4
	32 122.2	0.26	*wi*	∘∘∘	∘∘∘		32 145.7	0.35	4.7	*GC*1	1
	32 115.4	1.00	1.7	C_{4v}	1		32 140.8	0.19	5.4	∘∘∘	*p*3
	32 108.2	0.24	*wi*	O_h	2		32 115.8	0.09	*wi*	C_{4v}	1
	32 103.8	0.23	*wi*	C_{3v}	3		32 112.3	0.08	*wi*	∘∘∘	∘∘∘
	32 095.3	0.23	*wi*	O_h	1		32 109.0	0.08	*wi*	∘∘∘	∘∘∘
	32 094.8	0.22	*wi*	∘∘∘	∘∘∘		32 108.0	0.08	*wi*	∘∘∘	∘∘∘
	32 092.5	0.24	*wi*	∘∘∘	∘∘∘		32 105.2	0.08	*wi*	∘∘∘	∘∘∘
	32 091.0	0.23	*wi*	∘∘∘	∘∘∘		32 101.3	0.08	*wi*	∘∘∘	∘∘∘
	32 084.7	0.27	*wi*	∘∘∘	∘∘∘		32 092.2	0.30	3.9	∘∘∘	*p*2
	32 083.9	0.28	*wi*	*GC*2	∘∘∘		32 087.5	*wi*	*wi*	∘∘∘	∘∘∘
	32 081.7	0.30	*wi*	C_{3v}	2		32 086.8	*wi*	*wi*	∘∘∘	∘∘∘
	32 077.6	0.79	3.0	∘∘∘	*GC*		32 083.8	*wi*	*wi*	∘∘∘	∘∘∘
1.0	32 212.3	0.31	*wi*	*GC*2	∘∘∘		32 077.2	1.00	1.6	∘∘∘	*p*1
	32 209.6	0.31	*wi*	*GC*2	∘∘∘		32 073.6	0.09	*wi*	∘∘∘	∘∘∘
	32 204.5	0.34	*wi*	*GC*2	∘∘∘		32 072.3	0.09	*wi*	∘∘∘	∘∘∘
	32 158.4	0.53	*wi*	*GC*2	∘∘∘		32 056.1	0.06	*wi*	∘∘∘	∘∘∘
	32 148.8	0.37	*wi*	*GC*2	∘∘∘		32 055.0	0.06	*wi*	∘∘∘	∘∘∘
	32 124.9	0.54	*wi*	*GC*2	∘∘∘		32 017.1	0.07	*wi*	d	∘∘∘
	32 123.8	0.55	*wi*	*GC*2	∘∘∘		32 014.7	0.08	*wi*	d	∘∘∘
	32 119.1	0.65	*wi*	*GC*2	∘∘∘		32 012.8	0.11	3.1, *wi*	d	∘∘∘
	32 117.2	0.77	*wi*	*GC*2	∘∘∘		32 009.4	0.05	*wi*	d	∘∘∘
	32 107.9	0.40	*wi*	O_h?	2	1.0	32 189.9	0.39	*wi*	∘∘∘	∘∘∘
	32 098.2	0.56	*wi*	*GC*2	∘∘∘		32 188.6	0.39	*wi*	∘∘∘	∘∘∘
	32 094.5	0.63	*wi*	O_h?	1		32 175.5	0.40	*wi*	∘∘∘	∘∘∘
	32 089.8	0.76	*wi*	O_h?	∘∘∘		32 160.7	0.74	*wi*	∘∘∘	∘∘∘
	32 083.4	1.00	*wi*	*GC*2	∘∘∘		32 095.1	0.60	*wi*	∘∘∘	∘∘∘
	32 076.6	0.69	*wi*	*GC*2	∘∘∘		32 092.4	0.89	*wi*	∘∘∘	*p*2
	32 017.9	0.23	*wi*	d	∘∘∘		32 084.6	0.89	*wi*	∘∘∘	∘∘∘
	32 016.0	0.23	*wi*	d	∘∘∘		32 077.7	1.00	3.8	∘∘∘	*p*1

[a] Peak intensities relative to strongest peak for given excitation and given sample. Linewidths are full width at half maximum. *wi* indicates that either the line is too weak for measurement or there is too much interference from neighboring lines for a measurement. Cerium concentrations in mole percent.

[b] The dots indicate that there is no identification offered for this entry.

[c] Entries labeled *p*1, *p*2, etc., indicate that the line grows approximately as x^2.

[d] This entry is a low-wavenumber spectral line that was also observed by Smith and Yaney (Ref. 16) and/or Yaney and Donlan (Ref. 34) in singly doped SrF_2. See text.

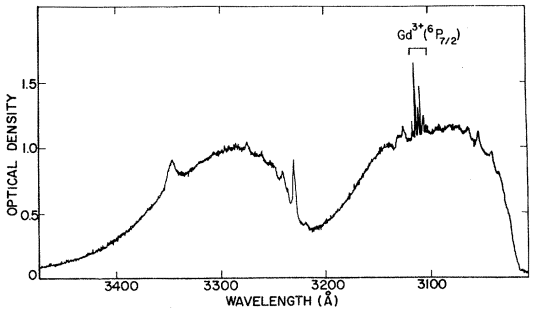

FIG. 7. Fluorescence spectrum of SrF_2 (0.1-mole % Gd^{3+} +0.01-mole % Ce^{3+}) at 77 °K. The broad bands are due to $5d \rightarrow 4f(^2F_{5/2}, {}^2F_{7/2})$ transitions of Ce^{3+}, and the unlabeled features on these bands are vibronic transitions after Kaplyanskii *et al.* (Ref. 31) and Loh (Ref. 32).

cant enhancement of the $^6P_{7/2}$ gadolinium fluorescence by the cerium. Secondly, there are two concentration ranges of enhancement, one in the 0.01–0.2%-Ce range and the other above 0.2%. Thirdly, the enhancement is essentially due to the new site *GC*1, which appears to be created when Ce is present. And finally, it is apparent that the C_{4v} fluorescence is at best, only slightly enhanced at Ce concentrations below 0.2% and quenched above this Ce level.

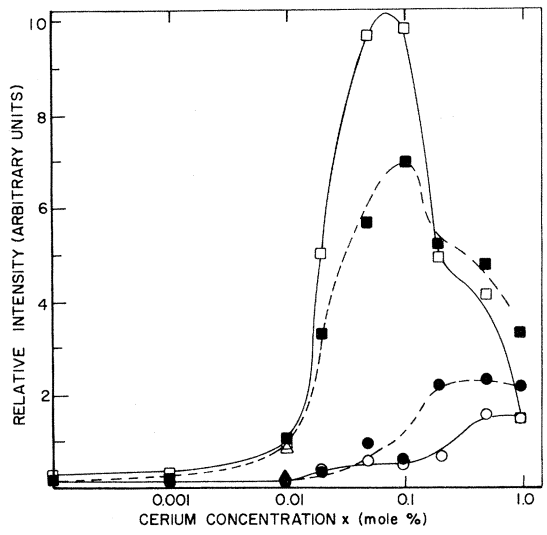

FIG. 8. Intensities of the total $^6P_{7/2}$ fluorescence of Gd^{3+} and the underlying 3100-Å fluorescence of Ce^{3+} for the SrF_2 (0.1-mole % Gd^{3+} + x-mole % Ce^{3+}) samples at 77 °K. At 2500-Å excitation—Gd^{3+} emission, □——; Ce^{3+} emission, ■---. At 2750-Å excitation—Gd^{3+} emission, ○——; Ce^{3+} emission, ●---. Values for 0.01% Ce^{3+} in SrF_2 for 2500- and 2750-Å excitations given by △ and ▲, respectively. Curves are hand fitted to show trends.

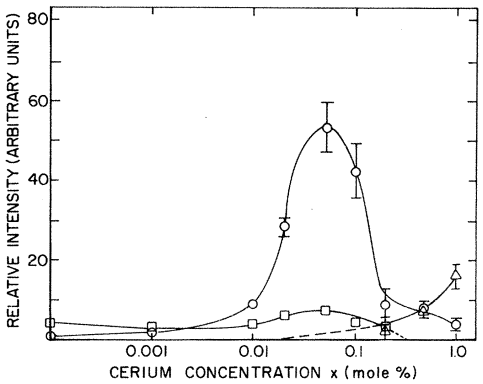

FIG. 9. Fluorescence intensities of the $^6P_{7/2}$ transitions of the C_{4v}, *GC*1, and *GC*2 lines of SrF_2 (0.1-mole % Gd^{3+} + x-mole % Ce^{3+}) at 77°K. Data were obtained line by line. Curves are hand fitted to show trends. Site C_{4v}, □; site *GC*1, ○; *GC*2 lines, △.

The remaining fluorescence data taken were the excitation spectra of select lines of the groups identified in Fig. 6 and Table III. The main objective was to help determine the possible origins of the *GC*1, *GC*2, *GC*, and *p* lines which are presumably due to mixed cluster sites containing at least one Gd ion, one Ce ion, and one or more interstitial fluorine F^-_{int} ions. The results of these measurements are summarized in Table IV. The proposal that Ce ions form clusters in the fluorites was first made by Loh.[32] He identified the absorption band just below 2500 Å in Fig. 4 as being due to the double clustering of Ce^{3+}-F^-_{int} in nearest-neighbor (nn) or next-nearest-neighbor (nnn) positions. In Table IV we see that the *GC*1 site is pumped by bands coincident with the Ce cluster bands. Thus, we conclude that the *GC*1 site is a double cluster consisting of one Gd ion, one Ce ion, and an unspecified number of F^-_{int} ions. Clearly, the *p* lines must have similar origins. The *GC*2 excitation spectrum was not studied because of the complexity of the fluorescence spectra at high Ce concentrations.

C. Lifetime data

The lifetimes of the fluorescence decay of the $^6P_{7/2}$ region (~3100 Å) were measured for 2750 and 2500-Å excitation at 77 and 300 °K for the nine doubly doped samples. From the fluorescence and excitation studies it is evident that for 2750-Å excitation and cerium concentrations less than 0.2%, the observed decays were due to the C_{4v} site. Above 0.2% concentration, the decay must be associated with the *GC*2 lines. With 2500-Å excitation, the decay clearly originates from the *GC*1 site and the *p* lines. The decay of the Ce fluorescence in this region was observed but was

TABLE IV. Fluorescence excitation peaks.

Fluorescence observed	Line [a]	Peak (Å)[b] 0.01%	0.1%	Probable origin [c]
Gd^{3+}	$C_{4v}(1)$	2390(*m*)	2390(*w*)	Ce doubles
Plus		2475(*w*)	2475(*s*)	Ce doubles
Ce^{3+}		• • •	2640(*w*)	*p* lines
		2740(*w*)	2740(*w*)	C_{4v}
	GC	• • •	2485(*s*)	*p*1
		• • •	2640(*s*)	*GC*, *p*1
	*GC*1(1)	2390	2390(*s*)	*GC*1, Ce doubles
		• • •	2475(*s*)	*GC*1, Ce doubles
		• • •	2640(*m*)	*p* lines
	*GC*2	• • •	~2750 [d]	?
Ce^{3+}	~3000 Å	• • •	2390(*w*)	Doubles
		• • •	2475(*m*)	Doubles
		• • •	~2980(*s*)	Singles

[a] See Fig. 6 and Table III.

[b] Wavelengths are to ±10 Å. The percentages are the molar values of the Ce^{3+} concentration in doubly doped SrF_2 samples having 0.1 mole % Gd^{3+}. The three dots specify either the peak was not observed or that the sample was not studied for the conditions indicated. Relative peak intensities within a given measurement are *w*, weak; *m*, medium; *s*, strong.

[c] See text.

[d] No study of the excitation spectrum of these lines was undertaken due to complexity of the fluorescence spectrum.

found to be limited to the 80-μsec minimum decay rate available with the equipment used. The results of these lifetime measurements of the $^6P_{7/2}$ state are plotted in Fig. 10. The decay of the *p*1 and *p*2 lines were observed to be the same as for the *GC*1 site, namely, 8.8 msec. We were not able to obtain a value for the *GC* line lifetime either due to a poor signal-to-noise ratio or because it was faster than our cutoff time.

The results obtained at 300 °K with 2750-Å excitation show a large scatter due to the low signal-to-noise ratio. In fact, the C_{4v} decay signal was too weak at the lower cerium concentrations to be measured. The 300 °K data taken with 2500-Å excitation were identical within experimental uncertainty, to the 77 °K data, and therefore are not shown. The 2500-Å values were essentially constant at 8.8 msec ±5%. An unexpected result shown in Fig. 10 is the large lifetime obtained for the C_{4v} site. As will be discussed in Sec. IV, the lifetime was lengthened by almost a factor of 4 over the radiative value obtained from the absorption spectra.

The fluorescence decay of the $^6I_{7/2}$ manifold of levels was also measured in four samples at 77 °K. This was accomplished, referring to Fig. 1, by exciting the high-lying ^6I states. Within uncertainty of the measurements, the four values were the same giving an average of 13.5 msec with an uncertainty of ±9%.

IV. ANALYSIS

A. *GC*, *GC*1, and *p*-Line site identities

Our objective here is to tie together the results cited herein and to firm up to the extent possible the various identifications and processes that have been alluded to. First of all, there is the question of the identity of the two new sites *GC* and *GC*1. If we accept Loh's proposal[32] that the 2440-Å band of Ce in SrF_2 is due to clustering of Ce^{3+}-F^-_{int} in double sites, then in view of the *GC*1 excitation

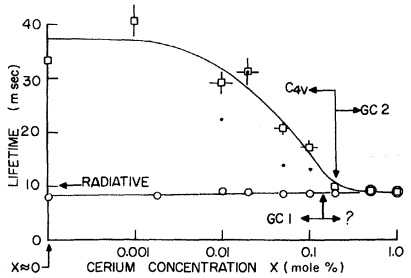

FIG. 10. Fluorescence lifetimes of the $^6P_{7/2}$ transitions of SrF_2 (0.1-mole % Gd^{3+} + *x*-mole % Ce^{3+}). Points □ are for 2750-Å excitation and ○ are for 2500 Å, both at 77 °K. The curve for the former is hand fitted and that for the latter is from a least-square fit. Points ● are for 2750 Å at room temperature. The radiative lifetime was determined from the C_{4v} absorption spectra. See Table V. See text concerning site labels.

TABLE V. Radiative lifetimes of the $^6P_{7/2}$, $^6I_{7/2}$, $^6D_{7/2}$, and $^6D_{9/2}$ states of Gd^{3+} computed from the oscillator strengths of the C_{4v} site in SrF_2. [a]

State	Lifetime (msec)
$^6P_{7/2}$	10
$^6I_{7/2}$	18
$^6D_{9/2}$	40
$^6D_{7/2}$	22

[a] Oscillator strengths after Detrio (Ref. 4).

spectra and the undeniable sharp four-line pattern of the 3100-Å fluorescence, we conclude that the $GC1$ site arises from the clustering of Ce^{3+}-F^-_{int} defect pairs with Gd^{3+}-F^-_{int} defect pairs to form mixed double sites. To do this we must rule out the possibility of absorption by the ^6D state of Gd. (See Fig. 1.) Table V gives the radiative lifetimes calculated from Detrio's[4] absorption oscillator strengths for Gd in the C_{4v} site of SrF_2. Comparing the C_{4v} fluorescence excited via the ^6I states to the possibility of the $GC1$ site strongly excited via the ^6D states, we see that this is clearly ruled out by the relative slowness of the ^6D lifetimes.

In order to lend additional support to the cluster thesis and to suggest an identification for the $GC1$ site, we calculated the concentrations of the single and double sites following the procedure used by Kreitman and Hamaker.[35] We make three basic assumptions. (i) The only effective interactions are nn and nnn interactions. (ii) The impurity ions are randomly distributed throughout the lattice. (iii) The presence of the interstitial fluorine ions does not influence the calculation. The second assumption neglects the additional charge on the impurity ions; therefore, the calculation should give at least a lower limit on cluster concentrations. The third assumption permits us to use the face-centered-cubic lattice as the basic structure of the system. The equations for concentrations of selected types of clusters are given in Table VI. These equations are plotted for our samples in Fig. 11. All other possible cluster sites have lower concentrations than those shown in Fig. 11 for our samples. We see that the two mixed double clusters D'_{xy} and D''_{xy} increase linearly with Ce concentration. Since the most probable mixed double is the nn cluster of Gd and Ce, we suggest this to be the identity of the $GC1$ site. Clearly, the energy transfer between the Ce and the Gd ions would be by exchange, which would explain the strong appearance of the $GC1$ site at low cerium concentrations. The natural

TABLE VI. Equations for concentrations of selected type of clusters in a face-centered-cubic lattice. [a]

Single	$S_x = xz^{18}$	$S_y = yz^{18}$
Pure double (nn)	$D_x = 12x^2z^{26}$	$D_y = 12y^2z^{26}$
Mixed double	$D'_{xy} = 12xyz^{26}$	$D''_{xy} = 6xyz^{30}$

[a] x and y are mole fractions of the two impurity ions, where $z \equiv 1-(x+y)$. D'_{xy} and D''_{xy} are nn and nnn mixed double clusters, respectively. See text.

identification for the GC site would then be the nnn mixed double cluster. However, the appearance of a single line in the $^6P_{7/2}$ spectrum presents a contradiction to the group-theoretical prediction. Therefore, either this line is not due to Gd at all or the value of J is not $\frac{7}{2}$. Values of $J=0$ or $\frac{1}{2}$ would produce a single line in all crystal-field symmetries. Thus, we are led to suggest that the GC line arises from a site containing a pair of Gd ions coupled so as to give such a value for J (at least to the first approximation). Since this line grows with the Ce concentration, we are further led to assume that the cluster also contains at least one Ce ion, which means that site is either a mixed triple site or a pair of mixed double clusters. Such sites are somewhat less probable than that calculated for the mixed double as described above. Needless to

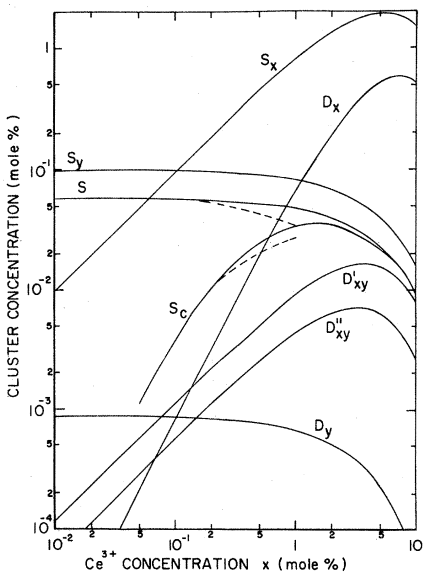

FIG. 11. Cluster site concentrations calculated for a doubly doped face-centered-cubic lattice. The solid curves labeled S and S_c are from the total and O_h curves in Fig. 5, respectively, with the dashed curves being from their experimental counterparts in Fig. 5. See Table VI for the identities of the remaining labels. See text for details of the calculations.

say, this line needs to be studied using the Zeeman effect of some other perturbation to clarify this situation. The observed dependence of the $GC1$ concentration on the Ce concentration is discussed in Sec. IV B.

The two mixed double clusters are shown in Fig. 12. The uncompensated symmetry of the nn mixed double site (viz., neglecting the F^-_{int} ions) is orthorhombic (C_{2v}). This symmetry is retained if the two nn interstitial positions common to the Gd and Ce ions are both occupied by F^-_{int} ions as shown in the figure. Such a configuration would appear to be energetically favored and would account for the narrowness of the $GC1$ lines. The presence of additional F^-_{int} ions or virtually any rearrangement of the two F^-_{int} ions would lower the symmetry to monoclinic. The uncompensated symmetry of the nnn mixed double site is tetragonal (C_{4v}). However, there are numerous configurations of two F^-_{int} ions which are energetically identical. Therefore, one would expect a basic tetragonallike line-splitting pattern but with the lines quite broad. This is what is observed of the four principal high-wavenumber lines in the $GC2$ group; however, such an identification is clearly speculative.

Pair lines, as well as pure double clusters, increase in strength with the square of the ion concentration. This is shown in Fig. 11 for the pure cerium double cluster D_x. Therefore, if we plot the ratio of the strengths of lines believed to belong to clusters containing two Ce ions to the strengths of lines belonging to single Ce sites, we should obtain a curve linearly dependent on the singles concentration which we assume is proportional to the Ce concentration. Such plots are given in Fig. 13 for the $p1$ line. These plots suggest that either the $p1$ line is due to a pair of $GC1$ sites or that it is due to Gd-Ce-Ce triple clusters. Among the remaining lines that are seen under 2500-Å excitation of the 0.1%-Ce sample in Fig. 6 five qualitatively grow at the same rate as the $p1$ line and are, therefore, tentatively identified as arising from Gd-Ce clusters containing two Ce ions.

The relative line strength of the GC line is also plotted in Fig. 13. Since the C_{4v} fluorescence intensity is proportional to the fractional site fraction ϵ times the observed lifetime τ_F, then if we take the ratio of the GC line strength to the $C_{4v}(1)$ line strength and multiply by $\epsilon\tau_F$ obtained from Figs. 5 and 10 for the C_{4v} site, we obtain a number proportional to the GC intensity divided by the Gd concentration. (For convenience we multiplied by $\epsilon\tau_F/\tau_R$, where τ_R is the radiative lifetime of 10 msec.) Thus, if the sample-to-sample Gd concentration is reasonably constant and if the τ_F and the actual τ_R for the GC line is independent of Ce concentration, then the resulting

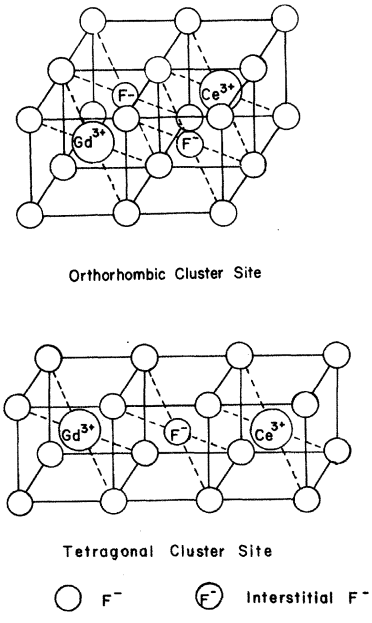

FIG. 12. Proposed Gd^{3+}-Ce^{3+} cluster sites in SrF_2. The position of a second F^-_{int} ion in the tetragonal cluster must be along the tetragonal axis, otherwise the symmetry is reduced to monoclinic. See text.

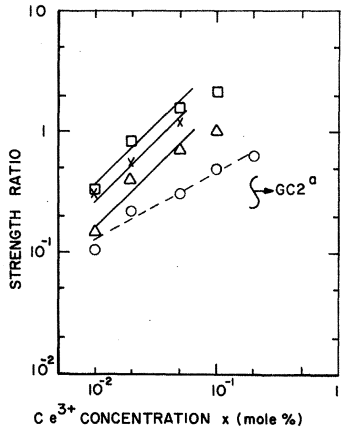

FIG. 13. Strength ratios of selected spectral features obtained from the SrF_2 (0.1-mole % Gd^{3+} + x-mole % Ce^{3+}) samples. Fluorescence line strength ratios of $p1$ to $GC1(3)$, □; $p1$ to $GC1(1)$, △; GC to $C_{4v}(1)$ times $\epsilon\tau_F/\tau_R$ (see text), ○; all of Gd^{3+} at 77 °K. See Fig. 6, Table III, and text concerning above line labels. Absorption strength ratio of the 2440-Å band to the 2950-Å band of Ce^{3+} at room temperature, ×. See Fig. 4. Solid lines have unity slope. The broken line is a least-squares fit (see text). (a) See Fig. 9 and text.

plot gives the GC-site-concentration dependence on the Ce concentration. This plot is given in Fig. 13 which, for a linear least-squares fit, has a slope of $0.57 \pm 10\%$. Although the Ce concentration functional dependence is approximately the square root rather than linear, the plot permits only a single Ce ion in the GC cluster. Thus, we are led to speculate that the GC site is a Gd-Gd-Ce triple.

In addition, Fig. 13 shows the plot of the band strength ratios of the 2440-Å band to the 2950 Å, both of Ce. This plot supports Loh's identification[32] of the 2440-Å band as being due to Ce clusters, in particular double clusters, and thereby lends further support to the assertion that Gd-Ce double clusters form at low Ce concentrations.

B. Excitation and decay schemes

The scheme proposed for the C_{4v} site is the usual three-level scheme with the uppermost level (pump level) being of the ^6I manifold and the intermediate level being of the $^6P_{7/2}$ manifold. Basically, the excitation is to the higher-lying states of the ^6I manifold, namely the $^6I_{9/2,17/2}$ and the $^6I_{11/2,15/2,13/2}$ states shown in Fig. 1. These levels decay by nonradiative transitions to the $^6I_{7/2}$ levels which are observed to fluoresce to the ^8S ground state. The average of the observed lifetimes of this transition was 13.5 msec. In addition, these levels decay nonradiatively to the ^6P state which then fluoresces at a rate dependent on the Ce concentration as given in Fig. 10. This is in qualitative agreement with the study of Gilfanov *et al.*[36] They reported the $^6I \rightarrow {}^8S$ and the $^6P \rightarrow {}^8S$ lifetimes to be about 8 and 9 msec, respectively. The latter agrees with the values we obtained with 2500-Å excitation. The discrepancy of the former with our results is probably due to the fact that since they did not spectrally resolve a given site in their measurements, their measurements were not of the C_{4v} site alone.

In our lifetime measurement setup, the excitation pulse duration was 16.7 msec. Because of the very long lifetimes observed for the $^6P_{7/2}$ fluorescence from the C_{4v} site at low Ce concentrations, we observed a rise in the ^6P fluorescence intensity from 3 to 7 msec (depending on the sample) after the excitation cutoff. A good review of this circumstance has been given by DiBartolo.[37] The times of this intensity maximum t_{max} were calculated[38] for three samples using the observed lifetimes and were found to agree with the observed values of t_{max} to within ±10%, thereby confirming the decay scheme.

The nonradiative decay rate of the $^6I_{7/2}$ levels to the ^6P state is the difference between the observed decay rate and the radiative decay rate. The radiative value from Table V is $(18 \text{ msec})^{-1}$, which gives [when subtracted from $(13.5 \text{ msec})^{-1}$] a nonradiative lifetime of 54 msec. This is in excellent agreement with what would be expected from Weber's study[39] for a nomial 3700-cm^{-1} separation between the pump and fluorescent levels.

The observed lifetimes of the $^6P_{7/2} \rightarrow {}^8S$ transitions in the C_{4v} site at 77 °K were found to approach the radiative value given in Table V at high Ce concentrations and to increase by up to almost a factor of 4 at low Ce concentrations. At 300 °K, the lifetimes followed roughly the same trend except that the values were lower for the most part, presumably due to increased coupling with the vibrating lattice. The mechanism which probably underlies the lengthening of the observed lifetime over the radiative value is radiation trapping. Inbusch[40] examined the radiation trapping mechanism in $Al_2O_3(Cr^{3+})$ and found the observed lifetime to exceed the radiative value by up to a factor of 4, depending on the Cr^{3+} concentration.

Briefly, the radiation trapping mechanism requires the existence of both single-ion and paired-ion sites. In addition, the samples must be large enough to permit the process to occur. In the excitation of the metastable state, radiation is normally emitted from single-ion sites as fluorescence decay. But in radiation trapping, single-ion sites decay from their metastable state either directly or stepwise through other single-ion sites into ion-pair states which are close in energy to the single-ion levels. The ion-pairs then fluoresce to their ground state. Energy transfer of this type is precluded, unless nonradiative coupling through ion-lattice interactions is available. Inasmuch as we did not do a Gd-concentration study with this double doping, it is not possible to unambiguously identify Gd-pair sites; however we have observed a number of low-wavenumber lines growing rapidly in the fluorescence spectra of Gd (singly) doped samples with Gd concentration.[34] These lines are identified by the letter d in Fig. 6 and Table III. Assuming that the appearance of radiation trapping signifies the existance of Gd-pair sites and that lowering the C_{4v} site concentration ϵ should reduce the lengthening of τ_F,[40] then since τ_F falls more rapidly than ϵ with Ce concentration, we are led to suggest that the GC line might be from Gd pairs combining with Ce to form Gd-Gd-Ce triples as previously suggested. That is to say, the Ce is extracting the Gd pairs faster than would be suggested from the C_{4v} concentration alone.

The decay scheme of the mixed clusters, in particular the GC and $GC1$ sites, are presumed to be primarily by exchange interactions directly from the Ce ion to the Gd ion and by superexchange

from the Ce to a F^-_{int} ion and then to Gd. The excitation is into the strong 5*d* bands of Ce. These mechanisms are in contrast to multipolar transfer by the fact that they are quite short range ($\lesssim$5Å).[41] For these sites, the Gd-Ce separation is constant; therefore, the efficiency of the energy exchange per site is independent of Ce concentration. On the other hand, multipolar energy transfer depends heavily on the activator-sensitizer separation,[42] and therefore their concentrations, as well as on the oscillator strengths of the activator and sensitizer transitions involved. The great dissimilarity of the Ce $4f \rightarrow 5d$ transition strengths, which are 10^{-2},[43,44] with the Gd $4f \rightarrow 4f$ transition strengths[4] (10^{-7}) makes multipolar energy transfer extremely weak. This was borne out to some extent by relative quantum-efficiency (QE) measurements made on our samples.[45] Taking the *GC*1 spectrum of the 0.5% sample (2500-Å excitation) as reference (relative QE equals unity), we calculated the QE's from the intensities of the *GC*1 and the C_{4v} plus *GC*2 fluorescence spectra (i.e., for the 2500 and the 2750-Å excitation cases). The calculation accounted for reabsorption of Gd fluorescence by Ce plus differences in quanta absorbed due to differences in Ce absorption and the excitation light intensity. The results are shown in Fig. 14. Any enhancement of the C_{4v} fluorescence would have to come via multipolar energy transfer. It appears in Fig. 14 that there is a loss of QE in the C_{4v} site due to increasing Ce. This apparent loss of observed QE arises because of the reduction in the radiation trapping phenomenon. This is shown in Fig. 14 where the C_{4v} QE is divided by the ratio of the fluorescence lifetime τ_F to the radiative lifetime τ_R resulting in a constant QE for the C_{4v} site over three samples. The increase in QE with the 0.01% sample suggests the possibility of energy transfer. Unfortunately, low Ce samples were not available when these measurements were made.

For the *GC* and *GC*1 sites, then, we expect the observed QE to follow the site concentration. If the assumptions used in arriving at the curves in Fig. 11 were strictly correct, then the *GC*1 plot in Fig. 14 would have unity slope. In actuality, the slope is $0.55 \pm 13\%$ by a least-squares fit. This means that the *GC*1 site concentration is proportional to approximately the square root of the Ce concentration. This is essentially the same dependence found for the *GC* line in Fig. 13. That the data follow a single relationship tends to support our analyses. That the slope is less than unity is consistent with the breakdown of the assumptions underlying Fig. 11. In the simplest terms, the additional repulsive energy due to the additional positive charges on the trivalent Ce and Gd ions in nn or nnn divalent metal ion positions would be

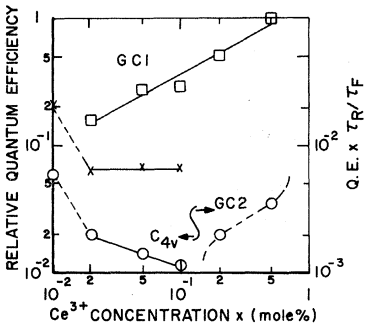

FIG. 14. Quantum efficiency of $^6P_{7/2}$ fluorescence transitions of Gd^{3+} in SrF_2 (0.1-mole % Gd^{3+} + *x*-mole % Ce^{3+}) at 77 °K obtained from intensity measurements. Excitation at 2500 Å, □, and 2750 Å, ○, refer to left-hand scale. The C_{4v} values are replotted, denoted by X, using the right-hand scale, where $\tau_R = 10$ msec from Table V and τ_F was obtained from Fig. 10. Solid lines are least-square fits.

expected to reduce the *growth rate* of the site below that predicted from a purely random distribution at low Ce concentrations. The data taken for the *GC*2 lines were insufficient to identify any well-defined behavior as observed for the *GC*1 site. Indications were that the QE increased rapidly above 0.5% Ce; however, the broad lines and the broad background present in the fluorescence spectra which appeared under 2750-Å excitation of the 0.5% and 1.0% Ce doubly doped samples and the lack of additional samples having higher Ce concentrations precludes a meaningful analysis of the *GC*2 lines in this paper.

C. Cubic site

Finally, let us examine the interesting behavior of the cubic-site concentration with increasing Ce concentration illustrated in Fig. 3 and plotted in Fig. 5. We will show that by accounting for the association energy of Gd^{3+}-F^-_{int} defect pairs, the dependence of Gd-singles concentration on total rare-earth (RE) concentration, and the probable stronger *gettering* action of Ce on F^-_{int} ions compared to that of Gd, we can explain reasonably well the observed Gd site concentration changes versus the Ce concentration.

It has been observed by several investigators[46] that as the RE impurity concentration is increased in fluorite crystals the relative number of cubic symmetry sites increases. This is exactly opposite to what one would expect on the basis of statistical mechanical considerations. A model has been proposed[28] which would resolve this discrepancy. The basic feature of the model is that a separate phase $RF_3{:}3(MF_2)$ (*R* is a rare-earth ion and *M* is a divalent metal ion) of a fluorite lattice

exists within the crystal which preserves a cubic environment for the tripositive RE ion, but for which the charge compensation mechanism is of a local nature. The usual compensation mechanism for cubic symmetry is of a nonlocal nature, i.e., the charge-compensating fluorine is so far away from the RE impurity that the point group symmetry of the RE site is the cubic symmetry of the fluorite lattice.[1] It is the relative populations of this type of site that one would expect to decrease as the impurity concentration is increased.

In the local cubic phase model R^{3+}-F^-_{int} defect pairs condense into the separate phase $RF_3{:}3(MF_2)$ by forming localized regions of high concentrations of these pairs. The point group symmetry of the RE impurity sites in this phase is cubic. As the concentration of RE impurities is increased more R^{3+}-F^-_{int} defect pairs condense into this phase, thus explaining the increase in the relative number of cubic impurity sites. Calculations performed by O'Hare[28] for the cases of $SrF_2(Gd^{3+})$ and $SrF_2(Gd^{3+}, Ce^{3+})$ indicated that the local cubic phase could form at concentrations as low as 0.36% total RE impurity concentration. However, he pointed out that this number is a rough approximation due to the many assumptions underlying his model. We would like to suggest that for the concentration range of $\lesssim 1\%$ there is no direct evidence for the existence of such a highly ordered cubic cluster. For concentrations above 1%, the studies of solid solutions of CaF_2 and YF_3 by Cheetham *et al.*[47] suggest that complicated clusters involving F^- ion vacancies are formed. Although they proposed no clusters having cubic symmetry, the possibility cannot be ruled out.

On the other hand, there is significant direct evidence that the degree of association of F^-_{int} ions with RE ions differs for different RE ions. Kristianpoller and Kirsh[48] showed in their studies of the ionic conductivity of singly doped SrF_2 containing Nd^{3+} and Tb^{3+} (< 1%) that the association between the Nd^{3+} ion and the F^-_{int} ion is somewhat stronger than between the Tb^{3+} ion and the F^-_{int} ion. This results in a smaller number of free F^-_{int} ions in the Nd^{3+}-doped samples. This is consistent with the earlier work of Brown *et al.*[49] who identify this decrease in association that occurs with increasing atomic number as being due to a decrease in the ionic radius.

A stronger association means a larger fraction of axial sites present in the sample, therefore leaving a smaller fraction of cubic sites. Thus, for our doubly doped samples we would expect that the Ce ions would all be in locally compensated axial sites, in particular, in the C_{4v} site as proposed by Loh,[32] whereas, the Gd ions would be in both cubic and axial sites. The latter is consistent with our observations for Gd in both singly[50] and doubly doped samples. (See Fig. 5.) If only one F^-_{int} is associated locally with each RE ion in an axial site, then as the RE concentration is increased, the single sites (viz., O_h, C_{4v}, C_{3v}) would all decrease by the same amount, as shown in Fig. 11 for S_y, regardless of the site symmetry. However, let us assume that a higher degree of association also means that there is higher probability for more than one F^-_{int} being associated with a given axial site. Thus, for our doubly doped samples this would mean that the Ce ions would tend to extract extra F^-_{int} ions from the Gd sites. This would of necessity have the effect of increasing the concentration of the usual cubic Gd sites. In other words, the Ce ions behave as a *gettering* agent for the F^-_{int} ions wherein, as the Ce concentration increases, the concentration of F^-_{int} ions involved in axial sites of Gd decreases and the O_h site concentration of Gd increases.

In order to give the gettering model analytical form, we make the two following assumptions. (i) The distribution of the Gd ions over the possible sites associated with that portion of the Gd population which, as it were, remains after the *gettering* effect of Ce is accounted for, is independent of the Ce concentration. In other words, we assume that the Gd ions in cubic sites introduced as the result of the Ce concentration are essentially extracted from the Gd population with the remaining ions being distributed among the possible sites as though the former were not there. It is as though the Gd concentration is reduced. Thus, for equal resultant Gd concentrations, the ratio of the Gd axial site concentration to the F^-_{int} concentration associated with the remaining Gd concentration is independent of the Ce concentration. For the low Gd concentration used in this work, we approximate this ratio as being independent of the resultant Gd concentration. (ii) The concentration of F^-_{int} ions associated with the remaining Gd ions decreases uniformly with increasing Ce concentration for constant Gd concentration.

Thus, we can write

$$S_g' = S_g [\, 1 + G_g(x) \,]^{-1} , \tag{6}$$

where S_g is the axial-site fractional molar concentration at zero Ce concentration ($x = 0$), S_g' is the concentration for $x \neq 0$, g identifies the site, and $G_g(x)$ is a single-valued monotonically increasing function of x. Following the statistical mechanical analysis of O'Hare,[28] the fractional concentration of a fluorine compensated axial site S_g is given approximately by

$$S_g = g S_y^2 / [g S_y + \exp(-|\epsilon_g|/kT)],$$

where $g = 6$ or 8 corresponds to either the C_{4v} or C_{3v} site, respectively, S_y is the fractional concentration of Gd ions in single sites, and ϵ_g is the association energy of the R^{3+}-F^-_{int} defect pair. The dependence of S_y on the dopant concentrations[35,45] x and y is given in Table VI. Thus, the net cubic concentration S_c is given by

$$S_c = S_y - \sum_g S'_g \ .$$

We chose $G_g(x)$ *ad hoc* to be

$$G_g(x) = \beta_g x^{\alpha_g} \ ,$$

where β_g and α_g are constants to be fitted. The result of fitting this calculation to the experimental site concentrations given in Table II is shown in Fig. 5. The following parameters were obtained. For C_{4v}: $\alpha = 1.5$, $\beta = 2.4$, and $-|\epsilon|/kT = -7.74$; and for C_{3v}: $\alpha = 1.5$, $\beta = 4.0$, and $-|\epsilon|/kT = -3.49$, where β is for x in percent. Considering the possible sample-to-sample differences in the actual total Gd concentrations, the fit is quite good. One of the parameters in the calculation to be fitted was the Gd concentration. The value shown in Fig. 5 for $x \approx 0$ corresponds to 0.057%. This choice was made to give approximately equal differences between the observed and calculated concentrations of the O_h and C_{4v} sites at $x = 1\%$.

Heist and Fong[1] have analyzed the distribution of M^{3+}-F^-_{int} defect pairs in fluorite-type lattices. Using their equilibrium temperature of 630°K, we obtain association energies of -0.42 and -0.19 eV for the C_{4v} and C_{3v} sites, respectively, which are to be compared to their values of -0.48 and -0.30 eV, respectively. The close agreement of the C_{4v} values gives some support to the correctness of the analysis. The discrepancy between the C_{3v} values is really not significant in view of the uncertainties in the C_{3v} data. The F^-_{int}-gettering parameter value of $\alpha = 1.5$ indicates that for Ce concentrations above 2.6%, an increase in the Ce concentration by $\frac{1}{3}$ will reduce the C_{4v} concentration by about $\frac{1}{2}$. At a Ce concentration of about 0.1%, an increase in the Ce concentration by $\frac{1}{3}$ will decrease the C_{4v} concentration by about $\frac{1}{20}$. Hence, the rate of loss of axial sites with increasing Ce concentration is greater than the rate of loss of Gd-singles concentration in the 0.1 to 1% range, resulting in the appearance and increasing concentration of the cubic sites.

Some insight into the proposed gettering mechanism is obtained from Fig. 11, where the O_h concentration S_c is plotted. We see that S_c follows very closely the Ce pure-double-cluster (nn) concentration D_x which suggests that it is the double-cluster sites which are responsible for the *gettering* action. Such a circumstance would provide a mechanism for self-gettering and thereby explain why the ratio of O_h to axial concentrations increases with increasing dopant concentration.[28] We believe this mechanism is consistent with the studies of Franklin.[51] In our optical studies of singly doped SrF_2 (Gd^{3+}) samples,[50] we find that the O_h site fraction increases to about 10% between 0.2 and 0.3% and remains essentially constant out to 0.5% while the C_{4v} site fraction starts decreasing at about 0.3% Gd. (This of course, means the O_h to C_{4v} ratio increases as reported from EPR studies.[27]) This slightly different behavior compared to that due to Ce can be attributed to a different degree of gettering action by the Gd population compared to Ce. Our thesis is that there are energetically favored clusters formed in RE-doped fluorites at low concentrations ($\lesssim 1\%$) which involve more F^-_{int} ions than required for local charge compensation. It is the essence of O'Hare's analysis[28] of this problem that complicated clusters can form at low concentrations which have a significant affect on the observed site distribution. The question to be answered is what are these clusters? The studies of Franklin[51] and Cheetham *et al.*[47] suggest that lattice F^- vacancies may play an important part in the formation of these clusters. Therefore, the gettering action may be due to F^- vacancy formation resulting from the dopant impurity rather than due directly to the impurity itself. In any case, there are numerous optical and EPR experiments that can be performed to help delineate these possibilities. Studies of doubly doped SrF_2 as performed here, except vs Gd concentration and with Ce replaced by Pr, Nd, and on through the RE series, would provide a rather definitive picture of the proposed gettering model as well as of the Gd-Ce line groups. Also, more refined calculations including third nn interactions as well as the association energies of the mixed clusters proposed herein would be helpful.

By far the most critical problem experimentally is the accuracy of the dopant concentrations and the absolute concentrations of the observed sites. The utility of optical studies of Gd is twofold. First of all, a self-consistent set of site fractions can be found due to the availability of transition oscillator strengths.[4,50] Secondly, the observed spectra are totally characteristic of the excited state because of the essentially unsplit ground state. The utility of Gd in SrF_2 is that the three basic fluorine-compensated sites O_h, C_{4v}, and C_{3v} appear at low Gd concentrations.

ACKNOWLEDGMENTS

The authors wish to thank V. L. Donlan, J. M. O'Hare, T. P. Graham, and J. A. Detrio for the many discussions, encouragements, references, and other assistances provided by them in the course of this work. One of us (P.P.Y.) wishes to recognize the faithful support of V. L. Donlan whose constancy permitted what amounted to insignificant ideas to mature into exciting happenings.

---

†This work was supported in part by the Air Force Materials Laboratory, Wright-Patterson Air Force Base, Ohio.

*Present address: Naval Electronic Systems Command, Washington, D. C. 20360.

‡Portions of this work were submitted in partial fulfillment of the requirements for Master of Science degrees at the University of Dayton.

§Present address: University of Northern Iowa, Cedar Falls, Iowa 50613.

[1]R. H. Heist and F. K. Fong, Phys. Rev. B 1, 2970 (1970), and references cited therein.

[2]J. M. O'Hare and V. L. Donlan, Phys. Rev. 185, 416 (1969).

[3]J. M. O'Hare, Phys. Rev. B 3, 3603 (1971).

[4]J. A. Detrio, Phys. Rev. B 4, 1422 (1971).

[5]R. Calvo, M. C. G. Passeggi, and M. Tovar, Phys. Rev. B 4, 2876 (1971).

[6]P. P. Yaney, Phys. Rev. B 9, 73 (1974).

[7]A. D. Franklin and S. Marzullo, Proc. Br. Ceram. Soc. 19, 135 (1971).

[8]J. B. Fenn, Jr., J. C. Wright, and F. K. Fong, J. Chem. Phys. 59, 5591 (1973).

[9]F. Z. Gilfanov, L. D. Livanova, A. L. Stolov, and Yu. P. Khodyrev, Opt. Spektrosk. 23, 431 (1967) [Opt. Spectry. 23, 231 (1967)], and previous papers cited therein.

[10]J. Makovsky, J. Chem. Phys. 46, 390 (1967).

[11]F. Z. Gilfanov, A. M. Leushin, and A. L. Stolov, Fiz. Tverd. Tela 9, 1357 (1967) [Sov. Phys.—Solid State 9, 1061 (1967)].

[12]J. A. Detrio, Phys. Lett. A 23, 82 (1968); Phys. Rev. 185, 494 (1969).

[13]P. P. Yaney (unpublished).

[14]M. W. Ferralli and P. P. Yaney, Bull. Am. Phys. Soc. 14, 798 (1969); M. W. Ferralli, M. S. thesis (University of Dayton, 1969) (unpublished).

[15]J. A. Detrio, M. W. Ferralli, P. P. Yaney, D. M. Ware, and V. L. Donlan, J. Chem. Phys. 53, 4372 (1970).

[16]W. K. Smith and P. P. Yaney, Bull. Am. Phys. Soc. 13, 958 (1968); W. K. Smith, M. S. thesis (University of Dayton, 1968) (unpublished).

[17]J. Sierro, Phys. Lett. 4, 178 (1963).

[18]H. W. Gandy and R. J. Ginther, Appl. Phys. Lett. 1, 25 (1962).

[19]L. D. Livanova, I. G. Saitkulov, and A. L. Stolov, Fiz. Tverd. Tela 11, 857 (1969) [Sov. Phys.—Solid State 11, 703 (1969)].

[20]G. E. Peterson and P. M. Bridenbaugh, Appl. Phys. Lett. 4, 173 (1964).

[21]J. E. Geusic, H. M. Marcos, and L. G. van Uitert, Appl. Phys. Lett. 4, 182 (1964).

[22]M. J. Weber, J. Appl. Phys. 44, 3205 (1973), and references cited therein.

[23]A. Bril, G. Blasse, A. H. Gomes de Mesquita, and J. A. de Poorter, Philips Tech. Rev. 32, 125 (1971), and references cited therein.

[24]V. L. Donlan (private communication).

[25]M. J. Weber, Solid State Commun. 12, 741 (1973).

[26]F. Z. Gilfanov, A. L. Stolov, and Zh. S. Yakovleva, Opt. Spektrosc. 23, 576 (1967) [Opt. Spectry. 23, 302 (1967)].

[27]G. K. Miner, T. P. Graham, and G. T. Johnston, J. Chem. Phys. 57, 1263 (1972).

[28]J. M. O'Hare, J. Chem. Phys. 57, 3838 (1972).

[29]Optovac Co., North Brookfield, Mass.

[30]Analyses performed by the Analysis Branch, USAF Materials Laboratory, Wright-Patterson Air Force Base, Ohio.

[31]A. A. Kaplyanskii, V. N. Medvedev, and P. P. Feofilov, Opt. Spektrosk. 14, 664 (1962) [Opt. Spectry. 14, 351 (1962)].

[32]E. Loh, Phys. Rev. 154, 270 (1967).

[33]B. R. Judd, Phys. Rev. 127, 750 (1962); also see B. G. Wybourne, *Spectroscopic Properties of Rare Earths* (Interscience, New York, 1965), Chap. 6.

[34]P. P. Yaney and V. L. Donlan (unpublished).

[35]M. M. Kreitman and F. Hamaker, J. Chem. Phys. 45, 2396 (1966).

[36]F. Z. Gilfanov, I. G. Saitkulov, and A. L. Stolov, Opt. Spektrosk. (Solid State Suppl.), 142 (1969) [Opt. Spectry. Solid State Suppl., 78 (1970)].

[37]B. DiBartolo, *Optical Interactions in Solids* (Wiley, New York, 1968), Chap. 18.

[38]D. M. Schaeffer and P. P. Yaney, Bull. Am. Phys. Soc. 15, 849 (1970); D. M. Schaeffer, M. S. thesis (University of Dayton, 1971) (unpublished).

[39]M. J. Weber, Phys. Rev. 157, 262 (1967).

[40]G. F. Imbusch, Phys. Rev. 153, 326 (1967).

[41]C. C. Klick and J. H. Schulman, in *Solid State Physics*, edited by F. Seitz and D. Turnbull (Academic, New York, 1951), Vol. 5, p. 119.

[42]D. L. Dexter, J. Chem. Phys. 21, 836 (1953).

[43]E. Loh, Phys. Rev. 147, 332 (1966).

[44]T. P. Pottenger and P. P. Yaney (unpublished).

[45]J. L. Wolf and P. P. Yaney, Bull. Am. Phys. Soc. 14, 799 (1969); J. L. Wolf, M. S. thesis (University of Dayton, 1969) (unpublished).

[46]See Ref. 23, and references cited therein.

[47]A. K. Cheetham, B. E. F. Fender, and M. J. Cooper, J. Phys. C 4, 3107 (1971).

[48]N. Kristianpoller and Y. Kirsh, Phys. Rev. B 4, 635 (1971).

[49]M. R. Brown, K. G. Roots, and J. M. Williams, J. Chem. Phys. 50, 891 (1969).

[50]P. P. Yaney (unpublished).

[51]A. D. Franklin (unpublished).